Available online at www.sciencedirect.com

ScienceDirect

Procedia Structural Integrity 39 (2022) 273–280

Structural Integrity Procedia

www.elsevier.com/locate/procedia

7th International Conference on Crack Paths

Prediction of multiaxial fatigue life of notched maraging steel components manufactured by selective laser melting

R. Branco[a]*, J.D. Costa[a], J. Jesus[a], F. Berto[b], J.A. Martins Ferreira[a], C. Capela[a,c]

[a]*CEEMPRE, Department of Mechanical Engineering, University of Coimbra, 3030-788 Coimbra, Portugal*
[b]*Department of Mechanical and Industrial Engineering, NTNU, 7491 Trondheim, Norway*
[c]*Department of Mechanical Engineering, ESTG, Instituto Politécnico de Leiria, 2411-901 Leiria, Portugal*

Abstract

This paper aims at predicting the fatigue crack initiation life in maraging steel manufactured by selective laser melting under in-phase bending-torsion loading. Three relationships between the bending moment and the torsion moment were studied, namely B/T=2, B/T=1, and B/T=2/3. The tested geometries consisted of hollow cylindrical specimens with lateral holes. The crack initiation and the crack paths were detected in-situ using a high-resolution digital camera. The local stress-strain states at the notch region were accounted for using two alternative numerical models developed within linear-elastic frameworks: (1) a parametric structured mesh; and (2) an automatic unstructured mesh. Fatigue crack initiation sites and fatigue crack initiation lives were successfully predicted using both numerical models.

© 2021 The Authors. Published by Elsevier B.V.
This is an open access article under the CC BY-NC-ND license (https://creativecommons.org/licenses/by-nc-nd/4.0)
Peer-review under responsibility of CP 2021 – Guest Editors

Keywords: multiaxial fatigue; fatigue crack initiation; maraging steel; selective laser melting

1. Main text

Maraging steels are a special class of advanced high-strength steels, widely used in the aircraft, aerospace, military, offshore, subsea, tooling and moulding industries due to the combination of unusual properties, namely high-strength,

* Corresponding author. Tel.: +351-239790700; fax: +351-239403407.
E-mail address: ricardo.branco@dem.uc.pt

2452-3216 © 2021 The Authors. Published by Elsevier B.V.
This is an open access article under the CC BY-NC-ND license (https://creativecommons.org/licenses/by-nc-nd/4.0)
Peer-review under responsibility of CP 2021 – Guest Editors
10.1016/j.prostr.2022.03.097

Nomenclature

a_0	crack initiation size
B/T	bending moment to torsion moment ratio
LM	line method of the Theory of Critical Distances
TCD	Theory of Critical Distances
SWT	Smith-Watson-Topper parameter
α_1, α_2	crack initiation angles at the hole surface
β_1, β_2	crack angles at the early stage of growth
σ/τ	normal stress to shear stress ratio
σ_{eq}	equivalent von Mises stress

toughness, ductility, and weldability, along with dimensional stability (Mooney, 2020; Branco, 2021). This special class of steels, whose microstructure is formed by a cubic martensitic matrix, is hardened by finely dispersed nanometer-sized precipitates of intermetallic compounds, formed from a metallurgical reaction involving no carbon, which seriously hampers the movements of dislocations and, thereby, promotes strengthening by precipitation hardening processes (Tan, 2017). Because of their martensitic matrix, these materials require a rapid quench from the austenitic region to temperatures below the martensite start temperature, which makes them particularly suited for selective laser melting (Tan, 2017; Mooney, 2020).

The development of reliable models for multiaxial fatigue life assessment is a complex task because, in general, there is a huge number of variables involved in the analysis (Carpinteri, 2008; Marciniak, 2008; Zhu, 2018; Cruces, 2019; Liao, 2020; Vantadori, 2021). Moreover, such a task is even more challenging for this new class of materials because they are highly susceptible to fatigue failure (Razavi, 2017; Fatemi, 2020; Garcias, 2021). The notch effect, particularly under multiaxial load histories, is a complex design problem (Berto, 2015; Zhu, 2020). It requires not only the knowledge about the crack initiation sites and direction of crack growth, but also an accurate evaluation of cyclic plasticity at the geometric discontinuities (Macek, 2017; Song, 2017).

The cyclic plasticity response at the geometric discontinuities is generally addressed by means of experimental techniques, numerical methods, or approximate solutions. Experimental techniques, due to their intrinsic nature, have some limitations, such as the difficulty to assess complicated geometric details, or the impossibility to analyse the stress-strain fields inside the body. In contrast, with the advent of computer technology, numerical methods allow to assess complex details not only at the surface, but also in depth (Zhu, 2018; Branco, 2020).

As far as the numerical methods are concerned, local stress-strain histories are generally computed considering elastic-plastic simulations or pseudo-elastic analyses (Macek, 2017; Pejkowski, 2019; Branco, 2021). Although, in theory, the former are more precise, the latter have the advantage of being faster and simpler, because they do not require complex constitutive models, nor too much computational time, while providing high efficiency (Susmel, 2007; Hu, 2019; Branco, 2021). Furthermore, constitutive relationships for additively manufactured maraging steel have only been derived for uniaxial loading (Antunes, 2019; Mooney, 2020a; Branco, 2021). Therefore, the development of simple methods able to assess the fatigue life under multiaxial loading for this new class of steels can be of great interest in a perspective of practical engineering design.

This paper compares two alternative models to predict the fatigue crack initiation sites and the fatigue crack initiation life in notched maraging steel manufactured by selective laser melting subjected to bending-torsion. These two approaches are based on the SWT damage parameter and account for the cyclic plasticity at the notch region by means of the finite element (FE) method. Both numerical models have a linear-elastic framework, but one is based on a structured mesh created with a parametric approach, while the other is based on an automatic unstructured mesh created with tetrahedral elements.

2. Materials and methods

The experimental tests were performed in hollow cylindrical geometries with lateral holes (see Fig. 1) made of maraging steel manufactured by selective laser melting. The specimens were manufactured using a Concept Laser M3

linear printing system equipped with a 400W Nd:YAG fibre laser. Each layer was created with a constant thickness of 40 μm, a scan speed of 200 mm/s, and a hatch spacing of 100 μm. After the additive manufacturing process, the 5mm-diameter hole was drilled by CNC, and the outer surface of the specimens was machined and polished to a scratch-free condition. The nominal chemical composition as well as the main mechanical properties are listed in Table 1 and Table 2, respectively. Three ratios of the bending moment to the torsion moment were studied, namely B/T=2, B/T=1, and B/T=2/3, which correspond to normal stress to shear stress ratios (σ/τ) equal to 4, 2 and 4/3, respectively. The tests were conducted for a stress ratio equal to 0. The hole surface was monitored in-situ to detect the crack initiation sites and track the crack paths during the tests (Branco, 2021).

Regarding the FE models, the two mesh topologies (near the geometric discontinuity) used to account for the cyclic plasticity at the notch-controlled process zone are exhibited in Figure 2. The structured mesh (Sm), developed in a parametric manner with 8-node hexahedral elements, is presented in Figure 2(a). The automatic unstructured mesh (Um), developed with 4-node tetrahedral elements, is displayed in Figure 2(b). The former contained 152,248 elements and 163,138 nodes, while the latter contained 642,821 elements and 906,676 nodes. Both modes assumed a homogeneous, linear-elastic, and isotropic behaviour. To reduce the computational overhead, at remote positions, coarser meshes were used. The bending moments and the torsion moments were generated by a single force applied in a prismatic arm with variable length connected to one end of the specimen, while the other end remained fixed.

Table 1. Chemical composition of maraging steel manufactured with a scan speed of 200 mm/s (Branco, 2018).

C	Ni	Mn	Co	V	Mo	Ti	Al	Cr	P	Si	Mn	Fe
0.01	18.2	0.65	9.0	-	5.0	0.6	0.05	0.3	0.01	0.1	0.04	Balance

Table 2. Mechanical properties of maraging steel manufactured with a scan speed of 200 mm/s (Branco, 2018).

Porosity (%)	ρ (g/m^3)	HV1	E (GPa)	σ_{UTS} (MPa)	σ_{YS} (MPa)	Strain at failure (%)
0.74±0.09	7.42	354±5	168±29	1147±13	910±11	5.12±0.001

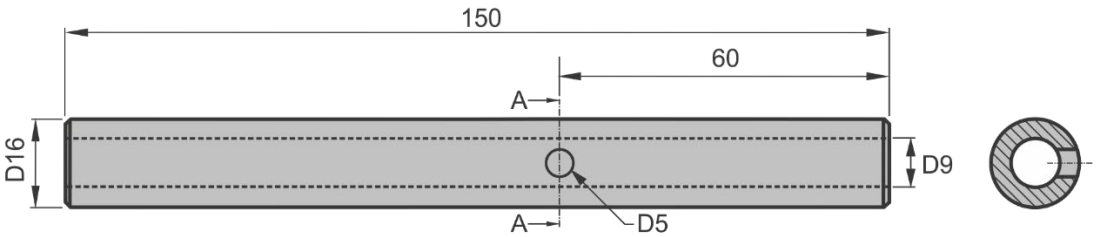

Fig. 1. Specimen geometry used in the bending-torsion tests.

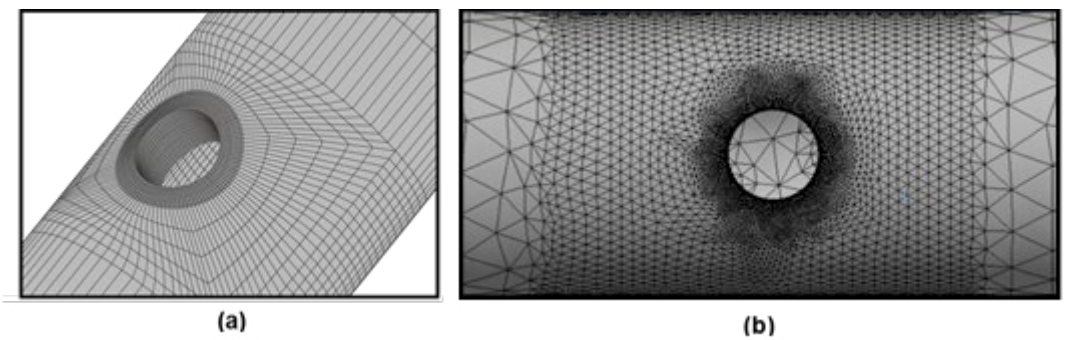

Fig. 2. Mesh topologies at the hole region: (a) structured mesh (Sm); and (b) unstructured mesh (Um).

3. Results

The typical appearance of fatigue crack paths and fatigue crack initiation sites is exhibited in Figure 3. In this geometry, under proportional bending-torsion loading, the fatigue process is characterised by the initiation and growth of two diametrically opposite cracks at the hole boundary. Overall, the two crack initiation sites observed in each test, defined by the β_1 and β_2 angles, maintained almost symmetrical positions relatively to a horizontal axis passing through the hole center (see Fig. 3). Regarding the crack angle at the early stage of growth, represented by the α_1 and σ_2 angles, the conclusions were similar, i.e. both angles were also relatively symmetrical with respect to a horizontal axis passing through the hole center (see Fig. 3). Not surprisingly, the bending moment to torsion moment ratio (B/T) had a strong effect on both the β angle and α angle. The increase of B/T ratio, which is associated with a reduction of the shear stress level, led to smaller values of the above-mentioned angles. As the B/T ratio increases, the fatigue propagation is closer to mode-I loading and, therefore, the degree of mixed-mode loading decreases.

A comparison between the experimental observations for the crack initiation angles (β_1 and β_2) and the numerical predictions obtained with the structured mesh (Sm) and the unstructured mesh (Um) is carried out in Figure 4. As can be seen in the figure, in general, the β angles increase with lower B/T ratios. These trends were also captured by both finite element models. Here, the initiation sites were predicted as the nodes at the hole boundary with the maximum

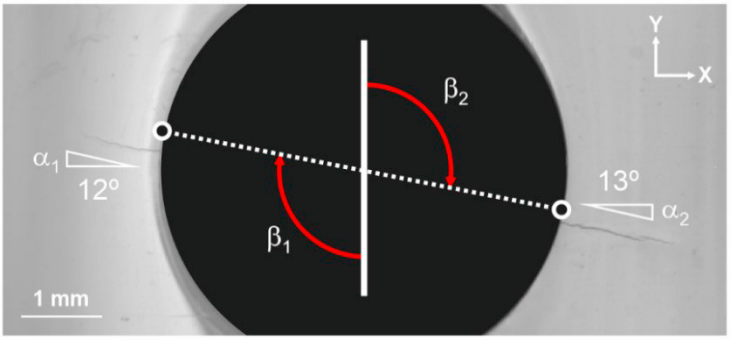

Fig. 3. Example of crack initiation sites and crack paths observed in the experiments for B/T = 2 ($\sigma/\tau = 4$).

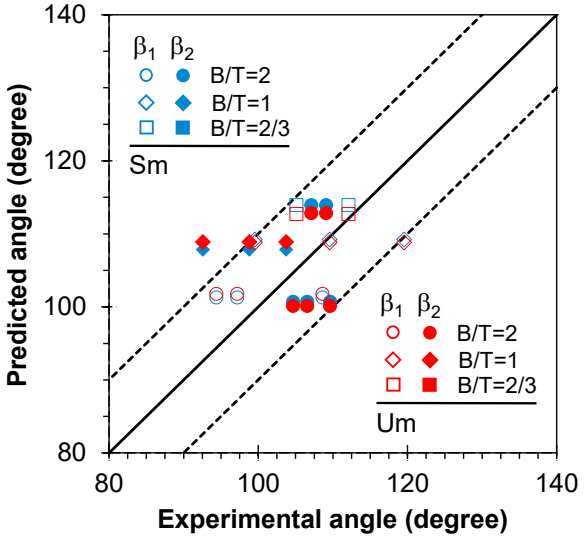

Fig. 4. Experimental fatigue crack initiation sites and predicted fatigue crack initiation sites obtained using both the structured meshes (Sm) and the unstructured meshes (Um).

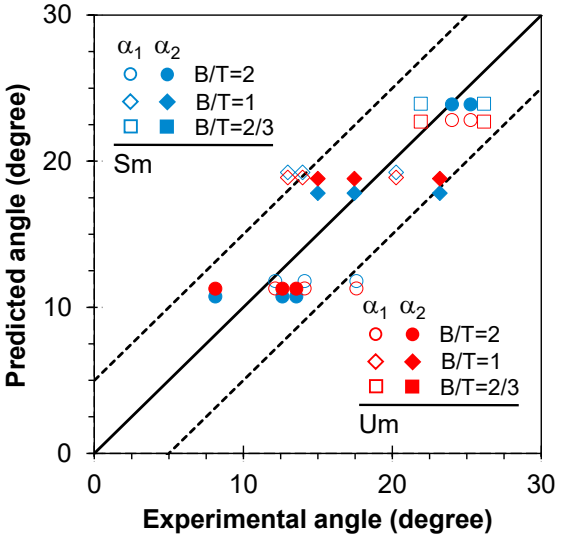

Fig. 5. Experimental fatigue crack angles and predicted fatigue crack initiation angles obtained using both the structured meshes (Sm) and the unstructured meshes (Um).

values of the first principal stress. It can be seen in the figure that the two FE models led to very similar predictions for the β_1 and β_2 angles. The maximum differences were lower than 2º (note that the blue and red symbols are almost overlapped). Moreover, most of points are within scatter bands of ±10º, which is an interesting outcome for additively manufactured steels subjected to multiaxial loading.

As far as the crack angles at the early stage of growth are concerned, the comparison between the experimental observations and the numerical predictions carried out using the two numerical models, i.e. the structured mesh (Sm) and the unstructured mesh (Um), can be seen in Figure 5. Again, we can conclude that both α angles increase with the reduction of the B/T ratio or, in other words, with the increase of the shear stress level. This behaviour was also captured by the two FE models. Here, the crack directions at the early stage of growth were estimated by computing the first principal direction of the nodes at the hole boundary with the maximum values of the first principal stress, i.e. at the crack initiation sites. As can be seen in the figure, these values are quite close to the experiments, with the maximum errors within scatter bands of ±5º, which is an interesting outcome. On the other hand, it is also clear that either the structured-based model or the unstructured-based model led to similar predictions with the maximum differences lower than 3º (note that the blue and the red symbols are almost overlapped).

In this study, the fatigue crack initiation life was assessed by means of the SWT-based model proposed by Branco et al. (2021). Briefly, the modus operandi consists of reducing the multiaxial stress state to an equivalent uniaxial stress state by computing the von Mises equivalent stress (σ_{eq}). The notch effect is accounted for by applying the Line Method (LM) of the Theory of Critical Distances (TCD). After calculating the effective von Mises equivalent stress range at the notch region, the Equivalent Strain Energy Density (ESED) concept is used to generate a cyclic stress-strain hysteresis loop representative of the loading scenario. Then, this strain hysteresis loop allows the calculation of the SWT damage parameter (Correia, 2017), which is then inserted into a uniaxial SWT-based fatigue master curve, obtained from smooth samples tested under strain-controlled conditions, to estimate the fatigue crack initiation life. The detailed formulation of the proposed model can be found in the recent paper by Branco et al. (2021).

The experimental fatigue crack initiation life was determined from the curves relating the crack length with the number of applied cycles, i.e. the well-known *a*-*N* curves, obtained from the images collected periodically during the tests with a high-resolution digital camera (similar to that of Figure 3). The crack initiation length (a_0) was defined via the El-Haddad parameter (El Haddad, 1979), with both constants (stress intensity factor range threshold and fatigue limit stress range) estimated for the stress ratio considered in the multiaxial fatigue campaign ($R = 0$). For the studied maraging steel manufactured by selective laser melting and tested under pulsating loading conditions, $a_0 = 121.7$ μm.

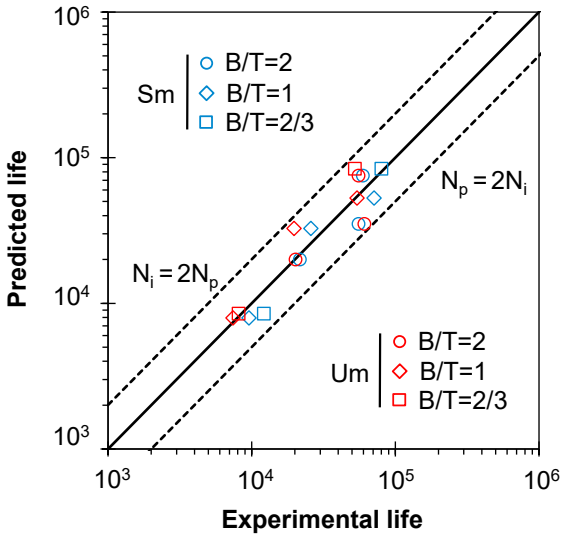

Fig. 6. Experimental fatigue crack initiation life versus predicted fatigue crack initiation life obtained using both the structured meshes (Sm) and the unstructured meshes (Um).

Figure 6 plots the experimental fatigue lives against the predicted fatigue lives for the structured mesh (Sm) and the unstructured mesh (Um). As can be seen in the figure, predictions are very well correlated with the experimental observations for the tested cases. All data points are within scatter bands with factors of ±2, which is an interesting outcome for additively manufactured steels subjected to multiaxial loading. Moreover, we can also distinguish that both numerical approaches (either the structured-based model or the unstructured-based model) led to similar results, which demonstrates the predictive capabilities of the proposed methodologies. Overall, the unstructured mesh led to slightly more conservative lives. Another important feature of the two approaches is the fact that they have a linear-elastic framework which makes them particularly attractive to industrial applications.

4. Conclusions

This paper compared the predictive capabilities of two different numerical models to determine the fatigue crack initiation sites, the fatigue crack directions, and the fatigue crack initiation life in maraging steel manufactured by selective laser melting subjected to bending-torsion. One numerical model was developed in a parametric manner based on a structured mesh, while the other was developed in an automatic manner based on an unstructured mesh. In both cases, the material was assumed as linear-elastic, homogeneous and isotropic. To validate the predicted results, experimental tests for a tubular cylindrical specimen with a transversal hole were performed. Three different bending moment to torsion moment ratios were considered, namely B/T = 2, B/T = 1, and B/T = 2/3. The tests were conducted under pulsating loading conditions under stress-control mode. The following conclusions can be drawn:

- The fatigue behaviour was characterised by the initiation of two cracks in diametrically opposite locations of the hole. These locations were relatively symmetrical to a line passing through the centre of the hole in a direction normal to the main axis of the specimen.
- The initiation sites were successfully predicted by the two numerical models for the different loading cases, with errors, in general, smaller than ±10º. Furthermore, the predictions obtained with the structured mesh and the unstructured mesh were very similar, with maximum differences lower than 2º.
- The crack directions in the early stage of growth were also similar for both sides of the hole, irrespective of the loading case. The predictions obtained with both numerical approaches led to maximum errors lower than ±5º. In addition, the differences between the structured mesh and the unstructured mesh were lower than 3º.

- Multiaxial fatigue life was successfully estimated by applying a SWT-based model, either for the structured mesh or the unstructured mesh, with all data points within scatter bands with factors of ±2. Although the results were relatively similar, the unstructured mesh led to slightly more conservative results.

Acknowledgements

This research is sponsored by FEDER funds through the program COMPETE – Programa Operacional Factores de Competitividade – and by national funds through FCT – Fundação para a Ciência e a Tecnologia – under the project UIDB/00285/2020.

References

Antunes, F., Santos, L., Capela, C., Martins Ferreira, J., Jesus, J., Prates, P. (2019). Fatigue crack growth in maraging steel obtained by selective laser melting. Applied Sciences 9, 4412.

Berto, F., Campagnolo, A., Lazzarin, P. (2015). Fatigue strength of severely notched specimens made of Ti–6Al–4V under multiaxial loading. Fatigue and Fracture of Engineering Materials and Structures 38, 503-517.

Branco, R., Costa, J.D., Martins Ferreira J.A., Capela, C., Antunes, F.V., Macek, W. (2021) Multiaxial fatigue behaviour of maraging steel produced by selective laser melting. Materials and Design 201, 109469.

Branco, R., Costa, J.D.M., Berto, F., Razavi, S.M.J., Martins Ferreira, J., Capela, C., Santos, L., Antunes, F.V. (2018). Low-cycle fatigue behaviour of AISI 18Ni300 maraging steel produced by selective laser melting. Metals 8, 32.

Branco, R., Prates, P.A., Costa, J.D., Borrego, L.P., Berto, F., Kotousov, A., Antunes, F.V. (2019). Rapid assessment of multiaxial fatigue lifetime in notched components using an averaged strain energy density approach. Int J Fatigue 124, 89-98.

Carpinteri, A., Spagnoli, A., Vantadori, S., Viappiani, D. (2008). A multiaxial criterion for notch high-cycle fatigue using a critical-point method. Engineering Fracture Mechanics 75, 1864–74.

Correia, J.A.F.O., Apetre, N., Arcari, A., De Jesus, A.M.P, Calvente, M., Calçada, R., Berto, F., Fernández-Canteli, A. (2017). Generalized probabilistic model allowing for various fatigue damage variables. Int J Fatigue 100, 187-194

Cruces, A.S., Lopez-Crespo, P., Bressan, S., Itoh, T., Moreno, B (2019). On the behaviour of 316 and 304 stainless steel under multiaxial fatigue loading: application of the critical plane approach. Metals 9, 978.

El Haddad, M.H., Topper, T.H., Smith, K.N. (1979). Prediction of non-propagating cracks. Engineering Fracture Mechanics 11, 573-584.

Fatemi, A., Molaei, R., Phan, N. (2020) Multiaxial fatigue of additive manufactured metals: Performance, analysis, and applications. Int J Fatigue 134, 105479.

Garcias, J.F., Martins, R.F., Branco, R., Marciniak, Z., Macek, W., Pereira, C., Santos C. (2021). Quasistatic and fatigue behavior of an AISI H13 steel obtained by additive manufacturing and conventional method. Fatigue and Fracture of Engineering Materials and Structures, https://doi.org/10.1111/ffe.13565

Hu, Z., Berto, F., Hong, Y., Susmel, L. (2019). Comparison of TCD and SED methods in fatigue lifetime assessment. International Journal of Fatigue 123, 105-134.
International Journal of Fatigue 152, 106459.

Liao, D., Zhu, S.P., Correia, J.A.F.O., De Jesus, A.M.P., Berto, F. (2020). Recent advances on notch effects in metal fatigue: A review. Fatigue and Fracture of Engineering Materials and Structures 43, 637-659.

Macek, W., Tadeusz, L., Mucha, R. (2017). Energy-based fatigue failure characteristics of materials under random bending loading in elastic-plastic range. Fatigue and Fracture of Engineering Materials and Structures 41, 249-259.

Marciniak, Z., Rozumek, D., Macha, E. (2008). Fatigue lives of 18G2A and 10HNAP steels under variable amplitude and random non-proportional bending with torsion loading. International Journal of Fatigue 30, 800-813.

Mooney, B., Agius, D., Kourousis, K.I. (2020a). Cyclic plasticity of the as-built EOS maraging steel: preliminary experimental and computational results. Applied Sciences 10, 1232.

Mooney, B., Kourousis, K (2020). A review of factors affecting the mechanical properties of maraging steel 300 fabricated via laser powder bed fusion. Metals 10, 1273.

Pejkowski, L., Skibicki, D. (2019). Stress-strain response and fatigue life of four metallic materials under asynchronous loadings: Experimental observations. International Journal of Fatigue 128, 105202.

Razavi, S.M.J., Ferro, P., Berto, F. (2017). Fatigue assessment of Ti–6Al–4V circular notched specimens produced by selective laser melting. Metals 7, 291.

Song, W., Liu, X., Berto, F., Wang, P., Xu, J., Fang, H. (2017). Strain energy density based fatigue cracking assessment of load-carrying cruciform welded joints. Theoretical and Applied Fracture Mechanics 90, 142-153,

Susmel, L., Taylor, D. (2007). A novel formulation of the theory of critical distances to estimate lifetime of notched components in the medium-cycle fatigue regime. Fatigue and Fracture of Engineering Materials and Structures 30, 567–81.

Tan, C., Zhou, K., Ma, W., Zhang, P., Liu, M., Kuang, T. (2017). Microstructural evolution, nanoprecipitation behavior and mechanical properties of selective laser melted high-performance grade 300 maraging steel. Materials and Design 134, 23-34.

Vantadori, S., Ronchei, C., Scorza, D., Zanichelli, A., Carpinteri, A. (2021). Fatigue behaviour assessment of ductile cast iron smooth specimens. International Journal of Fatigue 152, 106459.

Zhu, S.P., He, J.C., Liao, D., Wang, Q., Liu, Y. (2020). The effect of notch size on critical distance and fatigue life predictions. Materials and Design 196, 109095.

Zhu, S.P., Liu, Y., Liu, Q., Yu, Z.Y. (2018). Strain energy gradient-based LCF life prediction of turbine discs using critical distance concept. International Journal of Fatigue 113, 33-42.